Wideband saturable absorption in few-layer molybdenum diselenide (MoSe₂) for Q-switching Yb-, Er- and Tm-doped fiber lasers

R. I. Woodward,[1,†,*] **R. C. T. Howe,**[2,†] **T. H. Runcorn,**[1] **G. Hu,**[2]
F. Torrisi,[2] **E. J. R. Kelleher,**[1] **and T. Hasan**[2]

[1]*Femtosecond Optics Group, Department of Physics, Imperial College London, SW7 2AZ, UK*
[2]*Cambridge Graphene Centre, University of Cambridge, Cambridge, CB3 0FA, UK*
[†] *These authors contributed equally to this work.*
[*]*r.woodward12@imperial.ac.uk*

Abstract: We fabricate a free-standing molybdenum diselenide (MoSe₂) saturable absorber by embedding liquid-phase exfoliated few-layer MoSe₂ flakes into a polymer film. The MoSe₂-polymer composite is used to Q-switch fiber lasers based on ytterbium (Yb), erbium (Er) and thulium (Tm) gain fiber, producing trains of microsecond-duration pulses with kilohertz repetition rates at 1060 nm, 1566 nm and 1924 nm, respectively. Such operating wavelengths correspond to sub-bandgap saturable absorption in MoSe₂, which is explained in the context of edge-states, building upon studies of other semiconducting transition metal dichalcogenide (TMD)-based saturable absorbers. Our work adds few-layer MoSe₂ to the growing catalog of TMDs with remarkable optical properties, which offer new opportunities for photonic devices.

References and links

1. J. A. Wilson and A. D. Yoffe, "The transition metal dichalcogenides: discussion and interpretation of the observed optical, electrical and structural properties," Adv. Phys. **18**, 193 (1969).
2. P. B. James and M. T. Lavik, "The crystal structure of MoSe₂," Acta Cryst. **16**, 1183 (1963).
3. B. Evans and R. Hazelwood, "Optical and structural properties of MoSe₂," Phys. Stat. Sol. A **4**, 181 (1971).
4. J. M. Doviak and A. D. Yoffe, "Exciton-exciton interaction in MoSe₂ during laser irradiation," Phys. Lett. A **38A**, 59 (1972).
5. P. Joensen, R. F. Frindt, and S. R. Morrison, "Single-layer MoS₂," Mater. Res. Bull. **21**, 457 (1986).
6. C. B. Roxlo, R. R. Chianelli, H. W. Deckman, A. F. Ruppert, and P. P. Wong, "Bulk and surface optical absorption in molybdenum disulfide," J. Vac. Sci. Technol. A **5**, 555 (1987).
7. Q. H. Wang, K. Kalantar-Zadeh, A. Kis, J. N. Coleman, and M. S. Strano, "Electronics and optoelectronics of two-dimensional transition metal dichalcogenides," Nat. Nanotechnol. **7**, 699 (2012).
8. K.-G. Zhou and H.-L. Zhang, "Lighten the olympia of the flatland: probing and manipulating the photonic properties of 2D transition-metal dichalcogenides," Small, doi:10.1002/smll.201403385 (to be published).
9. K. F. Mak, C. Lee, J. Hone, J. Shan, and T. F. Heinz, "Atomically thin MoS₂: a new direct-gap semiconductor," Phys. Rev. Lett. **105**, 136805 (2010).
10. K. Wang, J. Wang, J. Fan, M. Lotya, A. O'Neill, D. Fox, Y. Feng, X. Zhang, B. Jiang, Q. Zhao, H. Zhang, J. N. Coleman, L. Zhang, and W. J. Blau, "Ultrafast saturable absorption of two-dimensional MoS₂ nanosheets," ACS Nano **7**, 9260 (2013).

11. K. Wang, Y. Feng, C. Chang, J. Zhan, C. Wang, Q. Zhao, J. N. Coleman, L. Zhang, W. Blau, and J. Wang, "Broadband ultrafast nonlinear absorption and nonlinear refraction of layered molybdenum dichalcogenide semi-conductors," Nanoscale **6**, 10530 (2014).

12. K.-G. Zhou, M. Zhao, M.-J. Chang, Q. Wang, X.-Z. Wu, Y. Song, and H.-L. Zhang, "Size-dependent nonlinear optical properties of atomically thin transition metal dichalcogenide nanosheets," Small **11**, 694 (2015).

13. Q. Ouyang, H. Yu, K. Zhang, and Y. Chen, "Saturable absorption and the changeover from saturable absorption to reverse saturable absorption of MoS_2 nanoflake array films," J. Mater. Chem. C **2**, 6319 (2014).

14. R. I. Woodward, R. C. T. Howe, G. Hu, F. Torrisi, M. Zhang, T. Hasan, and E. J. R. Kelleher, "Few-layer MoS_2 saturable absorbers for short-pulse laser technology: current status and future perspectives [Invited]," Photonics Res. **3**, A30 (2015).

15. S. Wang, H. Yu, H. Zhang, A. Wang, M. Zhao, Y. Chen, L. Mei, and J. Wang, "Broadband few-layer MoS_2 saturable absorbers," Adv. Mater. **26**, 3538 (2014).

16. H. Zhang, S. B. Lu, J. Zheng, J. Du, S. C. Wen, D. Y. Tang, and K. P. Loh, "Molybdenum disulfide (MoS_2) as a broadband saturable absorber for ultra-fast photonics," Opt. Express **22**, 7249 (2014).

17. R. I. Woodward, E. J. R. Kelleher, T. H. Runcorn, S. V. Popov, F. Torrisi, R. C. T. Howe, and T. Hasan, "Q-switched fiber laser with MoS_2 saturable absorber," in *CLEO:2014*, OSA Technical Digest (Optical Society of America, 2014), paper SM3H-6.

18. R. I. Woodward, E. J. R. Kelleher, R. C. T. Howe, G. Hu, F. Torrisi, T. Hasan, S. V. Popov, and J. R. Taylor, "Tunable Q-switched fiber laser based on saturable edge-state absorption in few-layer molybdenum disulfide (MoS_2)," Opt. Express **22**, 31113 (2014).

19. R. Khazaeinezhad, S. H. Kassani, T. Nazari, H. Jeong, J. Kim, K. Choi, J.-U. Lee, J. H. Kim, H. Cheong, D.-I. Yeom, and K. Oh, "Saturable optical absorption in MoS_2 nano-sheet optically deposited on the optical fiber facet," Opt. Commun. **335**, 224 (2015).

20. Z. Luo, Y. Huang, M. Zhong, Y. Li, J. Wu, B. Xu, H. Xu, Z. Cai, J. Peng, and J. Weng, "1-, 1.5-, and 2-um fiber lasers Q-switched by a broadband few-layer MoS_2 saturable absorber," J. Light. Technol. **32**, 4679 (2014).

21. H. Liu, A.-P. Luo, F.-Z. Wang, R. Tang, M. Liu, Z.-C. Luo, W.-C. Xu, C.-J. Zhao, and H. Zhang, "Femtosecond pulse erbium-doped fiber laser by a few-layer MoS_2 saturable absorber," Opt. Lett. **39**, 4591 (2014).

22. H. Xia, H. Li, C. Lan, C. Li, X. Zhang, S. Zhang, and Y. Liu, "Ultrafast erbium-doped fiber laser mode-locked by a CVD-grown molybdenum disulfide (MoS_2) saturable absorber," Opt. Express **22**, 17341 (2014).

23. B. Xu, Y. Cheng, Y. Wang, Y. Huang, J. Peng, Z. Luo, H. Xu, Z. Cai, J. Weng, and R. Moncorgé, "Passively Q-switched $Nd:YAlO_3$ nanosecond laser using MoS_2 as saturable absorber," Opt. Express **22**, 28934 (2014).

24. M. Zhang, R. C. T. Howe, R. I. Woodward, E. J. R. Kelleher, F. Torrisi, G. Hu, S. V. Popov, J. R. Taylor, and T. Hasan, "Solution processed MoS_2-PVA composite for sub-bandgap mode-locking of a wideband tunable ultrafast Er:fiber laser," Nano Res. **8**, 1522 (2015).

25. Y. Huang, Z. Luo, Y. Li, M. Zhong, B. Xu, K. Che, H. Xu, Z. Cai, J. Peng, and J. Weng, "Widely-tunable, passively Q-switched erbium-doped fiber laser with few-layer MoS_2 saturable absorber," Opt. Express **22**, 25258 (2014).

26. K. Wu, X. Zhang, J. Wang, X. Li, and J. Chen, "WS_2 as a saturable absorber for ultrafast photonic applications of mode-locked and Q-switched lasers," Opt. Express **23**, 11453 (2014).

27. D. Mao, Y. Wang, C. Ma, L. Han, B. Jiang, X. Gan, S. Hua, W. Zhang, T. Mei, and J. Zhao, "WS_2 mode-locked ultrafast fiber laser," Sci. Rep. **5**, 7965 (2015).

28. P. Yan, A. Liu, Y. Chen, H. Chen, S. Ruan, S. Chen, I. L. Li, H. Yang, J. Hu, and G. Cao, "Microfiber-based WS_2-film saturable absorber for ultra-fast photonics," Opt. Mater. Express **5**, 479 (2015).

29. S. H. Kassani, R. Khazaeizhad, H. Jeong, T. Nazari, D.-I. Yeom, and K. Oh, "All-fiber Er-doped Q-switched laser based on tungsten disulfide saturable absorber," Opt. Mater. Express **5**, 373 (2015).

30. S. Tongay, J. Zhou, C. Ataca, K. Lo, T. S. Matthews, J. Li, J. C. Grossman, and J. Wu, "Thermally driven crossover from indirect toward direct bandgap in 2D semiconductors: $MoSe_2$ versus MoS_2," Nano Lett. **12**, 5576 (2012).

31. J. N. Coleman, M. Lotya, A. O'Neill, S. D. Bergin, P. J. King, U. Khan, K. Young, A. Gaucher, S. De, R. J. Smith, I. V. Shvets, S. K. Arora, G. Stanton, H.-Y. Kim, K. Lee, G. T. Kim, G. S. Duesberg, T. Hallam, J. J. Boland, J. J. Wang, J. F. Donegan, J. C. Grunlan, G. Moriarty, A. Shmeliov, R. J. Nicholls, J. M. Perkins, E. M. Grieveson, K. Theuwissen, D. W. McComb, P. D. Nellist, and V. Nicolosi, "Two-dimensional nanosheets produced by liquid exfoliation of layered materials," Science **331**, 568 (2011).

32. G. W. Shim, K. Yoo, S.-B. Seo, J. Shin, D. Y. Jung, I.-S. Kang, C. W. Ahn, B. J. Cho, and S.-Y. Choi, "Large-area single-layer $MoSe_2$ and its van der Waals heterostructures," ACS Nano **8**, 6655 (2014).

33. J. C. Shaw, H. Zhou, Y. Chen, N. O. Weiss, Y. Liu, Y. Huang, and X. Duan, "Chemical vapor deposition growth of monolayer $MoSe_2$ nanosheets," Nano Res. **7**, 511 (2014).

34. X. Wang, Y. Gong, G. Shi, W. L. Chow, K. Keyshar, G. Ye, R. Vajtai, J. Lou, Z. Liu, E. Ringe, B. K. Tay, and P. M. Ajayan, "Chemical vapor deposition growth of crystalline monolayer $MoSe_2$," ACS Nano **8**, 5125 (2014).

35. Y. Zhang, T.-R. Chang, B. Zhou, Y.-T. Cui, H. Yan, Z. Liu, F. Schmitt, J. Lee, R. Moore, Y. Chen, H. Lin, H.-T. Jeng, S.-K. Mo, Z. Hussain, A. Bansil, and Z.-X. Shen, "Direct observation of the transition from indirect to direct bandgap in atomically thin epitaxial $MoSe_2$," Nat. Nanotechnol. **9**, 111 (2014).

36. N. Dong, Y. Li, Y. Feng, S. Zhang, X. Zhang, C. Chang, J. Fan, L. Zhang, and J. Wang, "Optical limiting of layered transition metal dichalcogenide semiconductors," arXiv:1503.02257 (2015).
37. Z. Luo, Y. Li, M. Zhong, Y. Huang, X. Wan, J. Peng, and J. Weng, "Nonlinear optical absorption of few-layer molybdenum diselenide ($MoSe_2$) for passively mode-locked soliton fiber laser [Invited]," Photon. Res. **3**, A79 (2015).
38. T. J. Mason and J. P. Lorimer, *Applied sonochemistry: Uses of power ultrasound in chemistry and processing* (Wiley-VCH, 2002).
39. C. M. Hansen, *Hansen solubility parameters* (CRC, 2007).
40. J. N. Coleman, "Liquid exfoliation of defect-free graphene," Acc. Chem. Res. **46**, 14 (2013).
41. G. Cunningham, M. Lotya, C. S. Cucinotta, S. Sanvito, S. D. Bergin, R. Menzel, M. S. P. Shaffer, and J. N. Coleman, "Solvent exfoliation of transition metal dichalcogenides: dispersibility of exfoliated nanosheets varies only weakly between compounds." ACS Nano **6**, 3468 (2012).
42. T. Hasan, F. Torrisi, Z. Sun, D. Popa, V. Nicolosi, G. Privitera, F. Bonaccorso, and A. C. Ferrari, "Solution-phase exfoliation of graphite for ultrafast photonics," Phys. Stat. Sol. B **247**, 2953 (2010).
43. A. R. Beal, J. C. Knights, and W. Y. Liang, "Transmission spectra of some transition metal dichalcogenides: II. Group VIA: trigonal prismatic coordination," J. Phys. C Solid State Phys. **5**, 3540 (1972).
44. Y. Li, A. Chernikov, X. Zhang, A. Rigosi, H. M. Hill, A. M. van der Zande, D. A. Chenet, E.-M. Shih, J. Hone, and T. F. Heinz, "Measurement of the optical dielectric function of monolayer transition-metal dichalcogenides: MoS_2, $MoSe_2$, WS_2, and WSe_2," Phys. Rev. B **90**, 205422 (2014).
45. M. Sheik-Bahae, A. A. Said, T.-H. Wei, D. Hagan, and E. Van Stryland, "Sensitive measurement of optical nonlinearities using a single beam," IEEE J. Quantum Electron. **26**, 760 (1990).
46. E. Garmire, "Resonant optical nonlinearities in semiconductors," IEEE J. Sel. Top. Quantum Electron. **6**, 1094 (2000).
47. N. Kumar, Q. Cui, F. Ceballos, D. He, Y. Wang, and H. Zhao, "Exciton-exciton annihilation in $MoSe_2$ monolayers," Phys. Rev. B **89**, 125427 (2014).

1. Introduction

Transition metal dichalcogenides (TMDs) are a family of more than 40 layered materials with general formula MX_2, where M is a transition metal, and X is a chalcogen (i.e. a group VI element such as sulfur or selenium) [1]. Their structure consists of quasi-2d layers weakly bound together by van der Waals forces. In each layer, a plane of transition metal atoms is covalently bonded between two planes of chalcogen atoms. TMDs have a diverse range of properties and include metallic (e.g. NbS_2), semiconducting (e.g. MoS_2) and insulating (e.g. HfS_2) materials [1].

Despite many fundamental studies of the structure and properties of TMDs in the 1960s and 70s [1–6], including reports of monolayer [5] and few-layer crystals [3], the lack of suitable processing and characterization techniques for such materials meant that their unique optical characteristics were not exploited for practical technologies. At present, semiconducting TMDs (MoS_2, $MoSe_2$, WS_2, WSe_2, $MoTe_2$ etc.) are experiencing renewed interest due to their remarkable layer-dependent optoelectronic properties, which hold great promise for future photonic devices [7]. These include a transition from an indirect to direct bandgap at visible / near-infrared wavelengths when moving from bulk to monolayer form, in addition to strong photoluminescence, high nonlinearity and ultrafast carrier dynamics for mono- and few-layer forms [7]. The direct bandgaps of monolayer semiconducting TMDs in the visible and near-infrared offer advantages over graphene, a zero-gap material, for many optoelectronic applications. Additionally, the layer- and size-dependent characteristics of these TMDs allow great flexibility for engineering their optical properties [7].

Molybdenum disulfide (MoS_2) is perhaps the most widely studied TMD to date [5–7, 9]. Recent work has demonstrated wideband saturable absorption in few-layer MoS_2 [10–13], suggesting that semiconducting TMDs could be a promising class of saturable absorber (SA) for short laser pulse generation [14]. Numerous studies have exploited this SA response, demonstrating mode-locked and Q-switched lasers (with both bulk and fiber gain media) from 1030 to 2100 nm [14–25] either at discrete wavelengths or with broadband tunability [16, 18, 25]. It has been proposed that the ability of a single MoS_2 SA device to operate at numerous wavelengths,

even in spectral regions corresponding to sub-bandgap photon energies, is due to edge-state absorption in the material [14, 18].

More recently, other *sulfide*-based TMDs such as tungsten disulfide (WS$_2$) have emerged as candidate materials for future saturable absorbers: WS$_2$ has recently been demonstrated to mode-lock and Q-switch fiber lasers [26–29]. However, *selenide*-based TMDs (MoSe$_2$, WSe$_2$, etc.) have yet to be fully explored and could offer advantages over sulfide TMDs for certain applications, for instance where a narrower gap semiconductor is required (heavier chalcogenide atoms lead to reduced bandgap energies [7, 8]). Therefore, further investigation to understand the optical properties of few-layer transition metal selenides is required before they can be exploited in practical systems.

Few-layer molybdenum diselenide (MoSe$_2$) flakes have been fabricated by mechanical exfoliation [30], ultrasound-assisted liquid-phase exfoliation (UALPE) [31] and chemical vapor deposition (CVD) [32–34] techniques. Bulk MoSe$_2$ has a $\sim$1.1 eV ($\sim$1128 nm) indirect bandgap, which increases to a $\sim$1.41 eV ($\sim$879 nm) indirect gap for 8-layer MoSe$_2$ [35] and a direct $\sim$1.55 eV ($\sim$800 nm) gap for monolayer MoSe$_2$ [30, 35]. The nonlinear optical properties of few-layer MoSe$_2$ have been studied by Wang et al. for UALPE MoSe$_2$ dispersed in cyclohexylpyrrolidone (CHP) [11], and by Dong et al. in N-methyl-pyrrolidone (NMP) [36]; both saturable absorption and optical limiting behavior were reported. During the review process, mode-locking of a fiber laser using few-layer MoSe$_2$ was reported [37], although only for operation at a single wavelength of 1558 nm.

Here, we produce a few-layer MoSe$_2$-polyvinyl alcohol (PVA) composite SA for short-pulse generation. Fiber lasers based on ytterbium- (Yb), erbium- (Er) and thulium-doped (Tm) gain media are demonstrated, operating at 1060 nm, 1566 nm and 1924 nm, respectively, which generate stable trains of Q-switched pulses when the MoSe$_2$-PVA SA is integrated into the cavity.
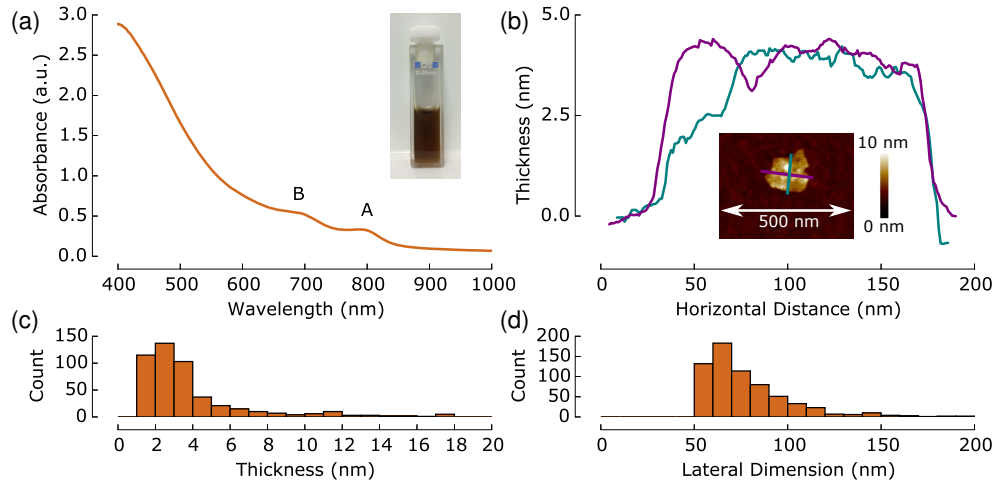

Fig. 1. (a) Linear optical absorption of MoSe$_2$ flakes in a 10% (v/v) dispersion, showing characteristic excitonic peaks (A & B) (inset: photograph of the diluted dispersion). AFM characterization of MoSe$_2$ flakes: (b) AFM image of a typical flake and two thickness profiles; (c) distribution of flake thicknesses; (d) distribution of lateral flake dimensions.

2. Few-layer MoSe$_2$ fabrication and integration into a saturable absorber device

We use an ultrasound-assisted liquid phase exfoliation (UALPE) technique to produce few-layer MoSe$_2$ nanoflakes from their bulk crystals. UALPE exploits cavitation arising from high frequency pressure variation. These microbubbles subsequently collapse due to instability, resulting in high shear forces [38]. This exfoliates flakes from bulk crystals by overcoming the interlayer van der Waals forces.

In general, solvents matching the experimentally-determined Hansen solubility parameters [39] of layered materials support their exfoliation and stabilization [40]. This offers a more refined understanding than considering only the surface energies or Hildebrand solubility parameters of the solvents and materials [40, 41]. Experimental evidence suggests that NMP and CHP are two of the more suitable solvents for TMDs [41]. However, it is challenging to process these high boiling point ($>150°$C) solvents for the fabrication of SA composites. Low boiling point solvents, e.g. water, are thus more desirable to exfoliate MoSe$_2$, although large mismatch of Hansen solubility parameters of water [39] with MoSe$_2$ (and other layered materials) [40] dictates the use of surfactants for its exfoliation and stabilization in water.

For layered materials, the molecular structure of surfactants plays an important role. The most effective are quasi-2d surfactants such as bile salts (e.g. sodium cholate) due to their planar structure with a hydrophobic and a hydrophilic side. The hydrophobic side of the bile salt surfactant molecules adsorbs onto the flat surface of the layered materials, while the hydrophilic side creates an effective surface charge around the flake [42]. The exfoliated layered materials are thus stabilized against re-aggregation by the Coulomb repulsion resulting from this surface charge. Among the different bile salt surfactants, we choose sodium deoxycholate (SDC) due to its high hydrophobic index [42]. We prepare the MoSe$_2$ dispersion by sonicating 100 mg of MoSe$_2$ crystals (Sigma Aldrich, 325 mesh) with 70 mg SDC (Sigma Aldrich, m.w. $\sim$1200-5000) in 10 mL deionized water for 12 hours at 15°C. The resultant dispersion is centrifuged at 4000 rpm ($\sim$1500g) for 1 hour to sediment the unexfoliated large flakes. The upper 70% of the centrifuged dispersion, enriched with few layer MoSe$_2$ flakes, is decanted for characterization and composite fabrication.

The optical absorption spectrum of the MoSe$_2$ dispersion, diluted to 10% (v/v) to avoid scattering losses, shows two absorption peaks labeled as A ($\sim$800 nm) and B ($\sim$710 nm) [Fig. 1(a)]. These peaks correspond to the excitons from the two spin-orbit split transitions at the K point of the Brillouin zone [43, 44]. To estimate the concentration of the dispersed MoSe$_2$, we use the Beer-Lambert law, $A_\lambda = \alpha_\lambda l c$, where A_λ is the absorbance at wavelength λ, α_λ is the absorption coefficient at λ, c is the concentration, and l is the optical path of incident light through the dispersion. First, we experimentally estimate α_λ for MoSe$_2$ at $\lambda =$710 nm following the procedure developed in Ref. [24] for MoS$_2$. This gives $\alpha_{710nm} = 615$ Lg^{-1}m^{-1}, from which we estimate the concentration of the undiluted MoSe$_2$ as 0.78 gL^{-1}.

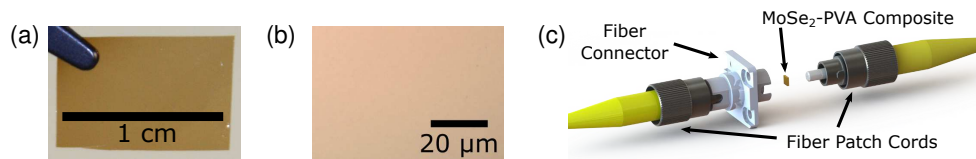The thickness distribution of exfoliated MoSe$_2$ flake dimensions is measured via atomic

Fig. 2. (a) Photograph of MoSe$_2$-PVA composite. (b) Optical micrograph showing absence of aggregates. (c) Schematic showing integration of MoSe$_2$ SA device between two fiber patch cords.
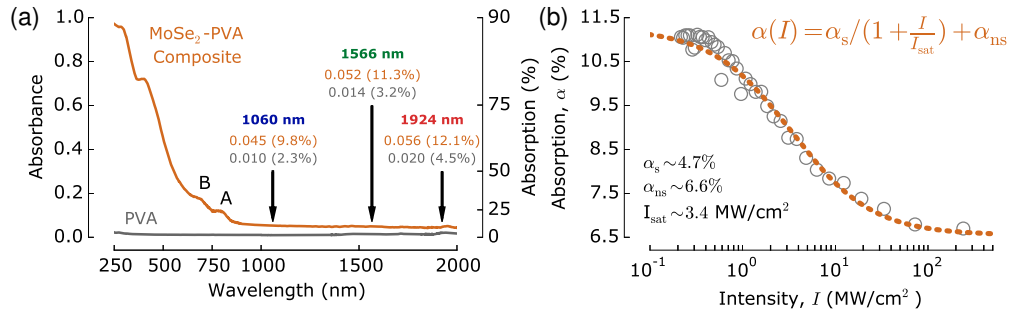
Fig. 3. Few-layer MoSe$_2$-PVA SA characterization: (a) linear optical absorption, with high-lighted absorption values at the operating wavelengths of our MoSe$_2$-based Q-switched lasers; (b) nonlinear optical absorption (at 1566 nm) measured by a Z-scan technique and well fitted by a two-level SA model [46],where α is absorption, I is incident intensity, α_s is modulation depth, α_{ns} is nonsaturable absorption and I_{sat} is saturation intensity.

force microscopy (AFM), shown in Figs. 1(b)–1(d). Samples for AFM are prepared by diluting the MoSe$_2$ dispersion to 5% (v/v), drop-casting on to a Si/SiO$_2$ wafer and then rinsing with deionized water to remove the surfactant. The average flake thickness is 3.8 ± 0.1 nm, while 80% of the flakes have thickness ≤ 5 nm [Fig. 1(c)], corresponding to ≤ 6–7 layers for the majority of the flakes, assuming 0.9–1.0 nm measured thickness for a monolayer flake [30], and 0.65–0.7 nm increase for each additional layer [35]. The average lateral dimension of the exfoliated flakes is 80 ± 5 nm, resulting in a high edge-to-surface area ratio [Fig. 1(d)].

The free-standing MoSe$_2$-polymer composite SA is fabricated by following a procedure commonly adopted for other layered material-based polymer composite SAs such as graphene [42] and MoS$_2$ [18, 24]. Briefly, 1.5 mL of the MoSe$_2$ dispersion is homogeneously mixed with 2 mL 5 wt% aqueous PVA solution. The mixture is poured into a petri dish and dried at room temperature in a desiccator. Slow evaporation of water over several days forms a $\sim$30 µm thick free-standing composite SA film [Fig. 2(a)]. An optical microscope image of the composite verifies the absence of aggregates and voids [Fig. 2(b)], which could otherwise increase the non-saturable scattering loss. For comparison, a $\sim$30 µm thick pure PVA film is fabricated using a similar method, but without the MoSe$_2$ flakes.

The linear optical absorption profile of the MoSe$_2$-PVA film shows the characteristic MoSe$_2$ excitonic peaks (A & B) and a non-negligible absorbance throughout the near-infrared ($>$800 nm), as highlighted in Fig. 3(a). The composite film absorption is $\sim$9.8%, $\sim$11.3% and $\sim$12.1% at 1060 nm, 1566 nm and 1924 nm, respectively (the three operating wavelengths of the lasers in Section 3), demonstrating a marked increase over the absorption values for the pure PVA film of $\sim$2.3%, $\sim$3.2% and $\sim$4.5%. The nonlinear optical response of the few-layer MoSe$_2$-PVA composite is measured using an open-aperture Z-scan technique [45]: the composite is swept through the focus of a beam of ultrashort pulses from a mode-locked fiber laser (750 fs pulse duration, 1566 nm wavelength, 7.5 MHz repetition rate) and the transmitted power is recorded as a function of incident intensity on the device (in addition to a reference power signal for normalization). Our few-layer MoSe$_2$ sample exhibits a strong saturable absorption response [Fig. 3(b)], well-fitted by the two-level SA model [46]. From this fit, the following SA parameters can be extracted: saturation intensity, $I_{sat} \sim 3.4$ MW/cm^2; modulation depth, α_s $\sim$4.7% and nonsaturable absorption, $\alpha_{ns} \sim 6.6\%$. Such SA parameters are similar in magnitude to previously reported saturable absorbers based on few-layer MoS$_2$ [14, 24]. We note that the Z-scan pulse source at 1566 nm corresponds to a photon energy of 0.79 eV, less than the energy

6

required for single photon excitation of carriers across the bandgap of few-layer MoSe$_2$ [30]. A proposal for the mechanism of the observed sub-bandgap saturable absorption is discussed in Section 3.4.

3. Q-switched fiber lasers using few-layer MoSe$_2$ SA

The demonstrated sub-bandgap saturable absorption of our few-layer MoSe$_2$-PVA composite at 1566 nm indicates that the device could Q-switch an Er-doped fiber laser cavity to generate short optical pulses, which are needed for many applications such as fundamental research and industrial materials processing and micromachining. The MoSe$_2$-PVA SA is integrated into an Er-doped fiber laser, in addition to Yb- and Tm-doped fiber lasers to explore the potential of exploiting sub-bandgap saturable absorption for short-pulse generation at different near-infrared wavelengths, using a single MoSe$_2$ SA. For each laser cavity, a ring design is adopted, including a polarization-independent isolator, output coupler and polarization controller, in addition to the fiber amplifier [Figs. 4(a), 5(a) and 6(a)]. The Yb and Er amplifiers consist of double-clad Yb and Er fiber, which are 1.5 m and 11.6 m long, respectively, pumped by multimode 965 nm laser diodes. The Tm fiber amplifier is formed of a 2.9 m length of single-clad Tm-doped fiber, pumped by a 1550 nm continuous wave fiber laser. The total lengths of the Yb, Er, and Tm fiber-based cavities are ∼15.9 m, ∼27.4 m and ∼13.4 m, respectively. A 1 mm × 1 mm piece of the MoSe$_2$ SA film is integrated into the cavity by placing it between two fiber patch cords [Fig. 2(c)].

3.1. Q-switched Yb:fiber laser characterization

Self-starting Q-switching is observed from the Yb-doped fiber laser, generating a steady train of pulses [typical pulse characteristics shown in Figs. 4(b) and 4(c)], centered at 1060 nm [Fig. 7(a)]. By changing the pump power, the average output power can be varied from 6.26 mW (corresponding to the threshold for Q-switched emission; below this, the laser output is a continuous wave) to 8.72 mW. The steady-state output pulse properties depend on the cavity gain and absorber saturation dynamics, coupling the pump power to the pulse duration and repetition rate. With increasing power, the pulse repetition frequency is increased from 60.0 kHz to 74.9 kHz and the duration decreased from 4.6 µs to 2.8 µs [Fig. 8(a)]. At the maximum average output power, the pulse energy is 116 nJ.

3.2. Q-switched Er:fiber laser characterization

The Er-doped fiber laser incorporating the few-layer MoSe$_2$-PVA composite exhibits self-starting Q-switching at an average output power of 18.9 mW, operating at 1566 nm [Fig. 7(b)]. Typical output pulse train properties are shown in Figs. 5(b) and 5(c). By varying the pump power, the repetition rate could be changed from 26.5 kHz to 35.4 kHz and the duration from 7.9 µs to 4.8 µs as the average output power increased from 18.9 mW to 29.2 mW [Fig. 8(b)]. At the highest output power, the pulse energy is 825 nJ.

3.3. Q-switched Tm:fiber laser characterization

Continuous-wave lasing at 1924 nm is initially observed as the pump power of the Tm-doped fiber laser is increased, until the Q-switching threshold is reached, corresponding to 0.13 mW average output power [Fig. 7(c)]. Beyond threshold, a steady train of Q-switched pulses is generated [Figs. 6(b) and 6(c)]. As the pump power is increased, the average output power increases and the Q-switched pulse duration reduces from 16.0 µs to 5.5 µs while the repetition rate increases from 14.0 kHz to 21.8 kHz [Fig. 8(c)]. The maximum pulse energy is 42 nJ.
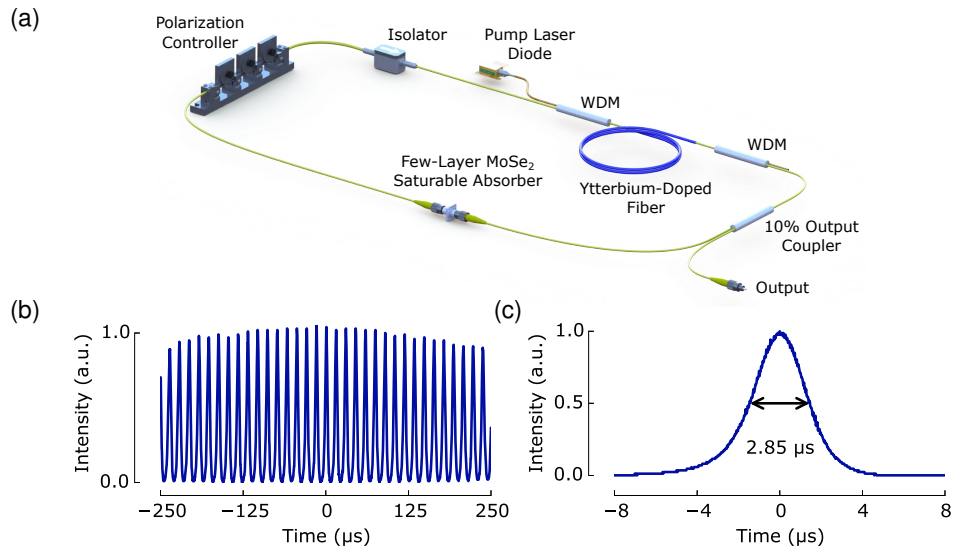
Fig. 4. Yb:fiber Q-switched laser: (a) cavity schematic; (b) output pulse train at 65.0 kHz repetition rate; (c) pulse profile with 2.85 µs duration for 8.0 mW average output power.

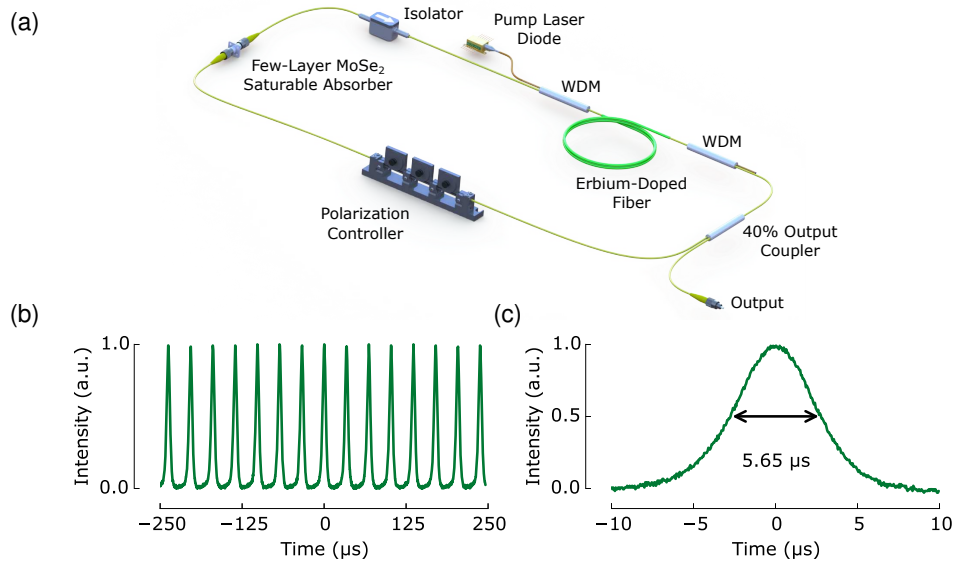

Fig. 5. Er:fiber Q-switched laser: (a) cavity schematic; (b) output pulse train at 29.4 kHz repetition rate; (c) pulse profile with 5.65 µs duration for 24.5 mW average output power.

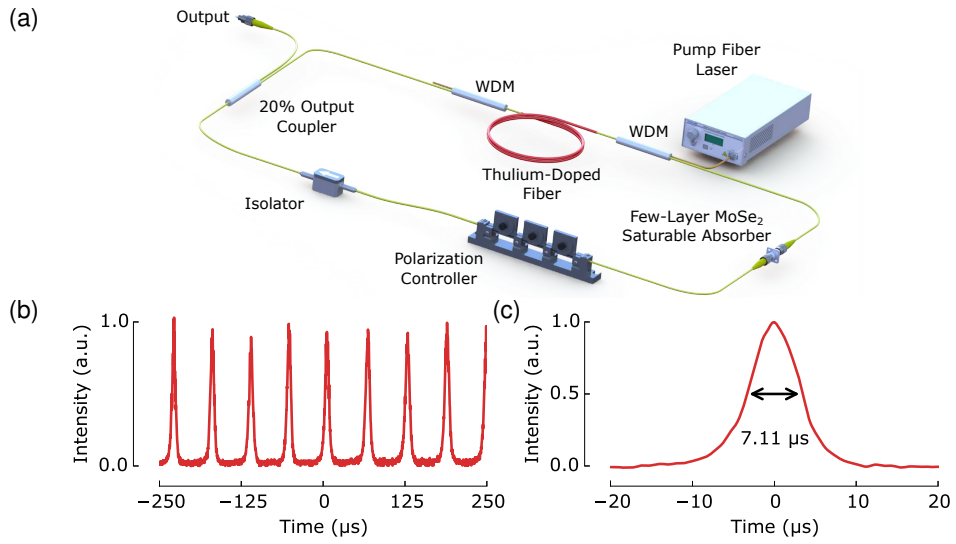Fig. 6. Tm:fiber Q-switched laser: (a) cavity schematic; (b) output pulse train at 16.9 kHz repetition rate; (c) pulse profile with 7.11 μs duration for 0.79 mW average output power.
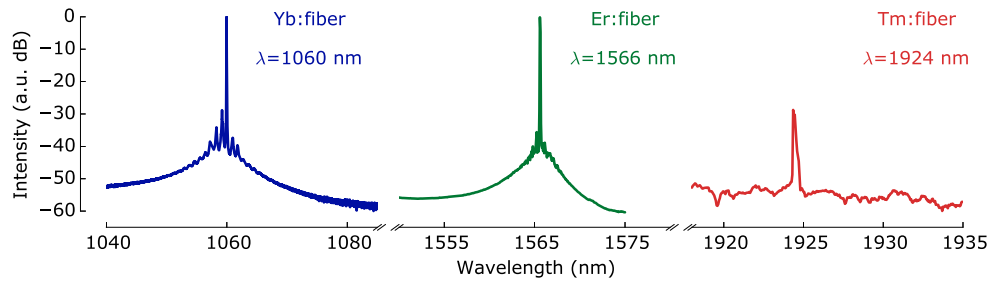

Fig. 7. Spectra for Q-switched operation of few-layer MoSe$_2$ Q-switched Yb- and Er- and Tm-doped fiber lasers; the Yb and Er spectrum were measured using an optical spectrum analyzer (0.02 nm resolution), while the Tm spectrum was measured on a spectrometer (∼0.1 nm resolution).
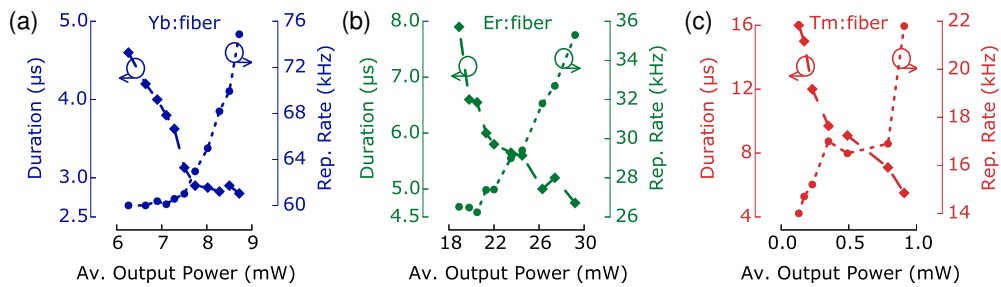

Fig. 8. Variation of pulse duration and repetition rate with average output power for (a) Yb-, (b) Er-, and (c) Tm-doped fiber lasers, Q-switched with a few-layer MoSe$_2$ SA.

9   Accepted for Optics Express, 10th June 2015

3.4. *Discussion*

The few-layer $MoSe_2$-PVA composite enables Q-switched operation in fiber laser cavities at 1060 nm, 1566 nm and 1924 nm. The lasers were also operated with $\sim$30 μm-thick pure PVA film (fabricated in a similar way to the $MoSe_2$-PVA composite, but without $MoSe_2$ flakes) sandwiched between the fiber patch cords, although in this case Q-switching was not observed at any power level or polarization controller position, confirming that the saturable absorption arises from the few-layer $MoSe_2$ material.

While bulk $MoSe_2$ has an indirect bandgap of $\sim$1.1 eV ($\sim$1128 nm) [30, 35], a recent angle-resolved photoemission spectroscopy (ARPES) study on molecular beam epitaxy (MBE)-grown $MoSe_2$ samples demonstrated a transition from an indirect bandgap of $\sim$1.41 eV ($\sim$880 nm) for 8-layer $MoSe_2$ to a direct bandgap of $\sim$1.58 eV ($\sim$784 nm) for monolayer $MoSe_2$ [35].

AFM statistics, considering $>$400 flakes of our UALPE $MoSe_2$ samples, show that 80% of the flakes consists of $\leq$6–7 layers. Based on the above experimental data and the ARPES study by Ref. [35], we estimate an indirect bandgap just above $\sim$1.41 eV for these flakes. Therefore, single-photon optical absorption from the few-layer $MoSe_2$ samples above 880 nm is not expected. However, our linear absorption measurement indicates $\sim$11% absorption at these near-infrared wavelengths ($>$880 nm), of which $>$70% ($\sim$8% absolute absorption) is due to the addition of $MoSe_2$ flakes, compared to the pure PVA film [Fig. 2(a)]. While this measurement could have also been affected by scattering loss, the sub-bandgap absorption observed in our UALPE $MoSe_2$ is verified by the Z-scan measurement at 1566 nm and demonstration of few-layer $MoSe_2$-based Q-switched lasers at 1060 nm (1.16 eV), 1566 nm (0.79 eV) and 1924 nm (0.64 eV). Indeed, similar observations of sub-bandgap saturable absorption have been reported for few-layer MoS_2 [10–24] and WS_2 [26–29].

We recently proposed an explanation for this phenomenon based on edge-states (in the context of MoS_2 SA devices) [14, 18, 24]. This mechanism is supported by early photothermal deflection spectroscopy studies of few-layer MoS_2 samples [6]. By comparing MoS_2 samples with different microcrystal sizes and lithographically textured single crystals, Ref. [6] demonstrated increased sub-bandgap absorption in samples with a greater amount of crystal edges. This suggests that states at the edges of the MoS_2 flakes play a significant role in defining the material band structure and enable absorption by exciting electrons to the edge-state levels within the material bandgap. This edge-induced sub-bandgap absorption can be saturated by Pauli blocking at high incident intensities, which enables the material to act as a Q-switch in a laser cavity [14, 18, 24]. We note that Wang et al. have also proposed a complementary explanation for this phenomenon, supported by theoretical bandgap studies, based on crystallographic defect states [15].

Generalizing the above discussion to other semiconducting few-layer TMD materials, we propose that a high edge-to-surface area ratio, can lead to sub-bandgap absorption in these materials. While this is not fully understood at present, crystallographic defects, dislocations, grain boundaries *etc* in semiconducting TMD samples may also contribute to sub-bandgap absorption. This could also explain observations of saturable absorption in CVD-grown MoS_2 samples [22], which, in general, are expected to have less edge-to-surface area ratio than those prepared by UALPE. Our UALPE $MoSe_2$ flakes with average lateral dimensions of 80 ± 5 nm have a high edge-to-surface area ratio, which we propose to be the primary origin of the optical absorption below the material bandgap.

Additionally, Kumar et al. recently reported absorption saturation in both bulk and monolayer $MoSe_2$ as part of a femtosecond transient absorption study, which they attributed to exciton-exciton interactions under intense pumping [47]. However, in this case the pump wavelength was 750 nm, tuned to the excitonic resonance. Therefore, while this excitonic mechanism may

contribute to saturable absorption at wavelengths corresponding to the bandgap, all three of our lasers operate at wavelengths with insufficient photon energies for resonant exciton excitation. Consequently, we believe that excitonic effects are not involved in the Q-switching of our lasers. Instead, we attribute the few-layer $MoSe_2$ intensity-dependent absorption to saturable edge states.

While the direct visible bandgap of monolayer and few-layer $MoSe_2$ suggests suitability for optical applications in the visible spectral region, the edge-state driven wideband absorption in the infrared highlights that few-layer $MoSe_2$ could be a very versatile material for developing future laser-based photonic technologies.

4.   Conclusion

In summary, we have reported the production of few-layer $MoSe_2$ flakes by ultrasound-assisted liquid-phase exfoliation and the fabrication of a saturable absorber device by embedding these $MoSe_2$ flakes into PVA. For the first time, we have demonstrated that a selenide-based transition metal dichalcogenide is able to generate short laser pulses by Q-switching: we developed ytterbium-, erbium- and thulium-doped fiber lasers, Q-switched by few-layer $MoSe_2$, operating at 1060 nm, 1566 nm and 1924 nm, respectively. The wideband saturable absorption was explained in the context of sub-bandgap edge states, extending our existing proposed mechanism for this phenomenon to the wider class of semiconducting transition metal dichalcogenides. This adds few-layer $MoSe_2$ to the growing library of nanomaterials with exceptional optical properties that offer exciting opportunities for future photonic applications.